# Automatic determination of white matter hyperintensity properties in relation to the development of Alzheimer's disease

Sandra van der Velden[a1], Christoph Moenninghoff[b], Isabel Wanke[b], Martha Jokisch[c], Christian Weimar[c], Rita Lopes Simoes[a], Anne-Marie van Cappellen van Walsum[d], Cornelis Slump[a]

[a] University of Twente, MIRA Institute for Biomedical Engineering and Technical Medicine, Drienerlolaan 5, Enschede, the Netherlands, 7522 NB; [b] University of Duisburg-Essen, University Hospital of Essen, Institute for Diagnostic and Interventional Radiology and Neuroradiology, Hufelandstrasse 55, Essen, Germany, 451 47; [c] University of Duisburg-Essen, University Hospital of Essen, Department of Neurology, Hufelandstrasse 55, Essen, Germany, 451 47; [d] Radboud University Medical Centre, Department of Anatomy, Geert Grooteplein Noord 21, Nijmegen, the Netherlands, 6525 EZ

## ABSTRACT

Alzheimer's disease (AD) is the most common form of dementia seen in the elderly. No curing medicine for AD exists at this moment. In the search for an effective medicine, research is directed towards the prediction of conversion of mild cognitive impairment (MCI) to AD. White matter hyperintensities (WMHs) have been shown to contain information regarding the development of AD, although non-conclusive results are found in literature. These studies often use qualitative measures to describe WMHs, which is time consuming and prone to variability. To investigate the relation between WMHs and the development of AD, algorithms to automatically determine quantitative properties in terms of volume and spatial distribution of WMHs are developed and compared between normal controls and MCI subjects.

MCI subjects have a significantly higher total volume of WMHs than normal controls. This difference persists when lesions are classified according to their distance to the ventricular wall. Spatial distribution is also described by defining different brain regions based on a common coordinate system. This reveals that MCI subjects have a larger WMH volume in the upper part of the brain compared to normal controls.

In four subjects, the change of WMH properties over time is studied in detail. Although such a small dataset cannot be used to give definitive conclusions, the data suggests that progression of WMHs in subjects with a low lesion load is caused by an increase in the number of lesions and by the progression of juxtacortical lesions. In subjects with a larger lesion load, progression is caused by expansion of pre-existing lesions.

**Keywords:** Alzheimer's disease, mild cognitive impairment, white matter hyperintensities, computer aided diagnosis, quantitative, automatic, MRI

## 1. INTRODUCTION

Alzheimer's disease (AD), the most common form of dementia, is a neurodegenerative disease often seen in the elderly. Guidelines for diagnosing AD consider the disease progression as a continuum, ranging from healthy ageing to preclinical AD, mild cognitive impairment (MCI) and finally dementia[1]. In the preclinical stage, neuropathological changes begin to emerge without affecting cognition yet[2]. MCI is considered to be the transitional period between normal cognitive function and dementia and can be subdivided into amnestic and non-amnestic MCI according to the presence of memory impairment. Not all patients with MCI will ultimately convert to AD, although patients with amnestic MCI have been found to be more likely to develop AD[3]. In the development of potential treatments and preventive therapies, it is important to distinguish between patients with MCI who will convert to AD and those who will

[1] Email: velden.sandra@gmail.com

Medical Imaging 2016: Computer-Aided Diagnosis, edited by Georgia D. Tourassi, Samuel G. Armato III,
Proc. of SPIE Vol. 9785, 97852D · © 2016 SPIE · CCC code: 1605-7422/16/$18 · doi: 10.1117/12.2216369

not. Therefore, research aims to develop diagnostic tools for patients with MCI and to distinguish MCI individuals that will convert to AD from those that will not.
Both volume and spatial distribution of white matter hyperintensities (WMHs) are being investigated in relation to MCI and AD. It has been shown that WMH volume increases rapidly in normal subjects developing MCI a decade later[4]. In a study by De Groot et al.[5], it is shown that severe periventricular lesions predict cognitive decline, whereas subcortical lesions are not related to cognitive decline. A recent study suggests that both the extent and location of WMHs are associated with the risk of MCI/dementia, with a high lesion load in the temporal region giving a significantly higher risk of developing MCI or dementia[6]. However, there is controversy regarding the relation between WMHs and the risk of developing MCI and AD, with several studies showing no relation between WMH volume and cognitive decline[7–9].
In this study, automated image analysis methods are developed in order to investigate the relation between WMHs and the development of dementia in a large (n = 190) cross-sectional cohort, using automatically determined, quantitative descriptors of WMHs in terms of volume and distribution. The same descriptors are used to investigate the progression of WMHs over time in a small (n = 4) longitudinal cohort.

## 2. METHODS

### 2.1 Data

At the University Hospital of Essen, Germany, a large nested case-control study is conducted. The main objective of this study is to investigate whether it is possible to predict which patients with MCI will convert to AD. At this moment, a total of 395 patients have been included. The data used in this papr is a subset of the data acquired in the Heinz Nixdorf Recall (HNR) study[10,11]. Participants with MCI are age, gender and education matched to cognitively normal subjects. All MR images were acquired at the University Hospital of Essen, Germany on a 1.5 T Siemens Avanto system. All participants were scanned with the same MR protocols. In this study, three-dimensional T1 images (TR = 40 ms; TE = 5 ms; voxel size = 1 $mm^3$), three-dimensional T2 images (TR = 3200 ms; TE = 413 ms; voxel size = 1 $mm^3$) and three-dimensional Fluid Attenuated Inversion Recovery (FLAIR) images (TR = 6000 ms; TE = 308 ms; TI = 2200 ms; voxel size = 1 $mm^3$) are used. Participants have received an MRI scan at baseline as well as a follow-up scan after 2.4 years.

A subset of 190 subjects (105 normal controls (NC), 82 MCI subjects) who received a FLAIR scan is used for cross-sectional analysis. Four subjects have received a FLAIR scan at baseline and at follow-up. Two subjects were diagnosed with pre-MCI and two subjects were diagnosed with MCI at baseline. None of the participants were diagnosed differently at follow up. These scans are used for longitudinal analysis. Subject demographics are shown in Table 1 and Table 2 (p-values lower than 0.05 are considered significant).

Table 1: Subject demographics of cross-sectional analysis for normal controls and mild cognitive impairment subjects.

| | **NC** | **MCI** | **p-value** |
|---|---|---|---|
| No. of participants | 105 | 82 | - |
| Females (%) | 54.3 | 45.1 | 0.358* |
| Age (y) | 71.32 ± 6.00 (57 – 82) | 72.33 ± 6.28 (55 – 83) | 0.191† |

* $\chi^2$-test
† Student's t-test

Table 2: Subject demographics of longitudinal analysis.

| **ID** | **Gender** | **Age at baseline (y)** | **Age at follow up (y)** | **Diagnosis** |
|---|---|---|---|---|
| 1 | Male | 63 | 69 | Pre-MCI |
| 2 | Male | 72 | 78 | Pre-MCI |
| 3 | Male | 56 | 59 | MCI |
| 4 | Female | 79 | 85 | MCI |

### 2.2 Lesion segmentation

Before the FLAIR images can be used for segmentation, the raw images are preprocessed. Preprocessing involves brain extraction and bias field correction. Since the segmentation method is fully intensity based, the skull and the brain stem,

which have similar intensities as the WMHs, have to be removed. Brain extraction is performed with the Brain Extraction Tool (BET)[12]. Subsequently, the images are bias field corrected using FMRIB's Automated Segmentation Tool (FAST)[13].
WMHs are segmented with the automatic segmentation algorithm of Lopes Simões et al.[14,15]. In short, the algorithm uses a context-sensitive Gaussian Mixture model to approximate the FLAIR histogram. A threshold is applied to this probability density map to segment the lesions. Finally, false positive segmentations due to FLAIR artefacts at the boundary between CSF and grey matter are removed. The resulting segmented lesions are used to determine the total volume and spatial distribution.

### 2.3 Volume

Total lesion volume is determined by summing over all segmented lesion voxels, multiplied by the voxel size. However, there is not only a natural variation in brain volume, shrinkage of the brain is a key symptom of AD. Therefore, total WMH volume is corrected for differences in brain volume by expressing it as percentage of total white matter volume. A white matter mask is created using the multichannel segmentation option of FAST[13]. Multichannel segmentation requires the T1 and T2 scans to be registered in a common space. To avoid interpolation errors in one of the two channels influencing the segmentation, both the T1 and the T2 scan are registered to the FLAIR image and masked with the FLAIR brain extracted volume. Registration is performed with FMRIB's Linear Image Registration Tool (FLIRT)[16,17]. Multichannel segmentation generates three binary masks: a cerebrospinal fluid mask, a grey matter mask and a white matter mask. The total white matter volume is obtained by summation over all voxels in the white matter mask and multiplication with the voxel size.

### 2.4 Spatial distribution

Spatial distribution of WMHs is quantified in two ways. Lesions are classified according to their distance to the ventricular wall and lesion volume in different parts of the brain is determined.

*Distance to the ventricular wall*
For the classification of WMHs in relation to their distance to the ventricular wall, the classification as proposed by Kim et al.[18] is used (Table 3). Juxtacortical lesions are not taken into account. The removal of false positives at the boundary between the grey matter and CSF might remove erroneously some of the juxtacortical lesions. Comparison of lesions in this subclass is therefore unreliable.

Table 3: Subclassification of WMHs as proposed by Kim et al.[18].

| | **Location** | **Etiology** | **Pathology** |
|---|---|---|---|
| Juxtaventricular | < 3 mm from ventricular wall | CSF leakage | Nonischemic |
| Periventricular | 3 – 13 mm from ventricular wall | Hypoperfusion | Ischemic |
| Deep | Between periventricular and juxtacortical | Small vessel disease | Ischemic |
| Juxtacortical | < 4 mm from corticomedullary junction | Small vessel disease | Ischemic |

To calculate the distance from the lesion voxels to the ventricular wall, the lateral ventricles are segmented from the image. The ventricles are extracted from the CSF mask created by the lesion segmentation algorithm. First, a region of interest proportional to the size of the brain and containing the lateral ventricles is applied to the CSF mask. Second, the mask is binary eroded to disconnect the lateral ventricles from other parts of the ventricular system. Finally, the components representing the lateral ventricles are selected and dilated back to their original size. Figure 1 shows an example of the result of the ventricle segmentation algorithm.

With the lateral ventricles segmented, the Euclidean distance of each WMH voxel to the ventricular wall is calculated. The lesions are then classified as juxtaventricular (within 3 mm of the ventricular wall), periventricular (between 3 and 13 mm of the ventricular wall) or deep (more than 13 mm of the ventricular wall). Lesion volume per class is obtained by summing all voxels in that particular class and multiplication with the voxel dimensions.

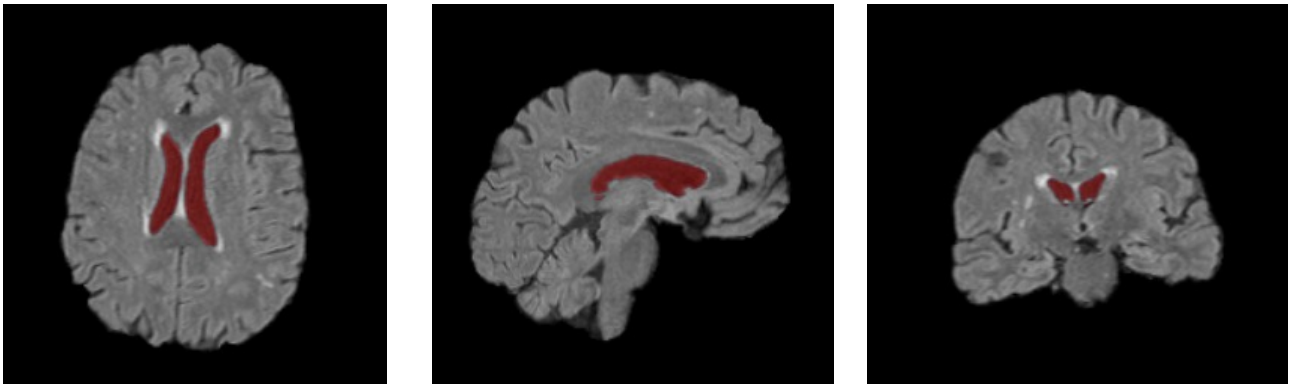

(a) (b) (c)

Figure 1: Example of ventricle segmentation in a brain with WMHs: (a) axial view, (b) sagittal view, (c) coronal view. The segmented ventricles are shown in red.

*Lesions in different brain regions*

To compare WMH location, lesion locations are expressed in an ideal head coordinate system. This ideal head coordinate system is defined with the origin in the centre of the brain with positive X0, Y0 and Z0 axes pointing in the right, anterior and superior directions, respectively. However, scans are oriented in a working coordinate system XYZ, in which X and Y are oriented with the rows and columns of each axial slice and Z is the actual axis of the scan. The working coordinate system is rotated over three angles (pitch angle ω, roll angle φ and yaw angle ϑ) with respect to the ideal coordinate system. These three angles are different for all scans and are dependent on the position of the patient in the scanner. By defining the yaw, roll and pitch angles, the location of each WMH can be expressed in the ideal coordinate system and compared between subjects.

The human brain is approximately bilateral symmetrical, as can be seen in axial and coronal slices. When the brain is aligned with the ideal coordinate system, the mid-sagittal (symmetry) plane is the Y0Z0-plane. However, the head is often tilted, resulting in non-zero yaw and roll angles. As a consequence, it is non-trivial to capture the mid-sagittal plane from a given set of axial or coronal slices. The method of Liu et al.[19] is used to extract the mid-sagittal plane and to obtain the roll and yaw angle.

The Talairach space is often used as a reference coordinate system. In this space, the intercommissural basal brain line is defined as the line passing through the superior edge of the anterior commisure (AC) and the inferior edge of the posterior commissure (PC)[20]. This line is used to determine the pitch angle. However, determination of this line without registration to an atlas is not possible. The corpus callosum, which is relatively easy to identify, has also been proposed as a reference system[20] and will be used in our method. The pitch angle is estimated by the orientation of the corpus callosum. This orientation is defined as the angle between the Y -axis and the major axis of the ellipse that has the same second-moments as the segmented corpus callosum. A schematic example is shown in Figure 2a.

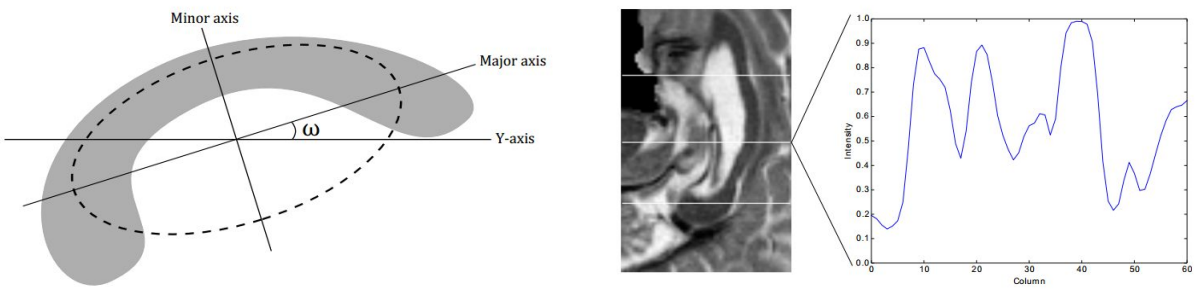


(a) (b)

Figure 2: Determination of the pitch angle. (a) Schematic of an ellipse with same second order moment as the corpus callosum. The pitch angle ω is defined as the angle between the Y -axis and the major axis of the ellipse. (b) The intensity profile along three rows (indicated with a white line) in the region of interest is taken to determine the local intensity of the corpus callosum. Going from left to right, the last local minimum lower than 0.3 is considered to be situated in the corpus callosum.

The corpus callosum is segmented on the sagittal slice embedding the centre of mass of the brain in the registered T2 scans. In a rectangular region of interest, histogram equalisation is used to enhance contrast, after which the image is thresholded. The intensity threshold $t_{cc}$ is found by examining intensity peaks along the central row of pixels, as well as along the rows at $1/4^{th}$ and $3/4^{th}$ of the number of rows in the region of interest. The last local minimum along this line lower than 0.3, is assumed to be situated in the corpus callosum. For each line, the intensity at this local minimum is found, giving an indication of the intensity of the corpus callosum (Figure 2b). To accommodate for variations in intensity, 0.1 is added to each local minimum. The mean intensity threshold $t_{cc}$ is defined as the mean of the three local thresholds. After removal of the background, the resulting largest component is eroded to remove spurious pixels. If the segmentation does not fulfil the segmentation criteria (e.g. corpus callosum is separated into two parts by the erosion), the segmentation procedure is repeated on a slice above and below the starting slice. If the criteria are still not fulfilled, the segmentation is repeated with a higher intensity threshold $t_{cc}$.

With pitch, yaw and roll angles determined, the location of each WMH in the working coordinate system is transformed to a location in the ideal coordinate system. Based on the signs of the coordinates in the ideal coordinate system, the brain is divided into eight octants (Figure 3). Per octant, the total volume of WMHs is determined.

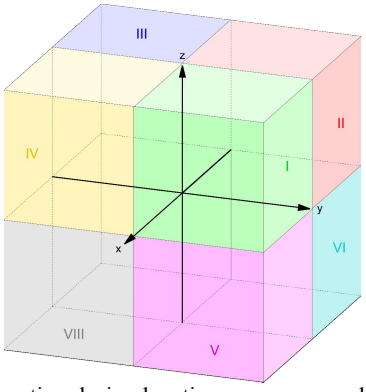


Figure 3: To compare WMH location, lesion locations are expressed in an ideal coordinate system. This ideal coordinate system is divided into eight octants. Adapted from [21].

### 2.5 Cross-sectional analysis

Group differences are evaluated with Student's t-test when a normal distribution is assumed. A $\chi^2$-test is used to evaluate group differences on a binomial scale. The Mann-Whitney-U test is used to test whether the two groups differ when data is not normal distributed. Correlation is evaluated with Spearman's correlation coefficient. Effects are considered statistically significant when $p < 0.05$.

### 2.6 Longitudinal analysis

*Registration*

In order to study the progression of WMHs, baseline and follow up scans of each subject are registered into a common space using FLIRT[16,17]. A rigid registration is performed with multiple resolution steps minimising the normalised cross-correlation between baseline and moving image. The transformation $T_{\mu}(\mathbf{x})$ is obtained by using the baseline scan as the reference image and the follow up scan as the moving image. Here, we define the common registration space as the average position of the baseline and follow up scan. Consequently, both scans are comparably deformed and interpolated when registered, thus avoiding errors based on registration of just one volume. Transformation matrices for the transformation of the baseline and follow up image volumes in the common space are then computed as $(\mathbf{I} + T_{\mu} - 1)/2$ and $(\mathbf{I} + T_{\mu})/2$, respectively, with $\mathbf{I}$ the identity matrix. When registering the baseline and follow up scans together, the WMHs should not influence the registration. Especially newly formed WMHs in the follow up scan might affect the registration. Therefore, both a baseline and follow up weighting volume is created. This weighting volume allows the cost function to have a different weighting at each voxel. By setting the weighting to zero at the WMHs, these voxels are not taken into account during the registration.

*Properties of WMHs*
In longitudinal analysis, the change of WMH properties is of interest. Any deviations from the previously described methods will be delineated here. The white matter volume mask used in the calculation of the total volume of WMHs, created from the T1 and T2 scan, has to be in the same common space as the FLAIR scan. Therefore, the transformation matrix to register to the original FLAIR scan is concatenated with the transformation matrix for registering the FLAIR scan to the common space. In this way, both the T1 and T2 scan are registered into the same common space as the FLAIR scan, so that the white matter mask lines up. Spatial distribution of the lesions is determined without any deviations.

Besides these properties, WMHs are tracked in baseline and follow up images, classifying them as matched, lost or new. Therefore, WMHs detected in baseline and follow up images are compared one-by-one. A lesion is classified as matched if a lesion detected at baseline is found within 3 mm from a lesion detected at follow up. This 3 mm encompasses possible small mistakes in registration and lesion segmentation. New lesions are WMHs only appearing in the follow up volume, lost WMHs are lesions only found at baseline.

Since only a small dataset is available (n = 4), no statistical tests are performed. Instead, the change of the various properties over time per subject is presented. This gives an indication of the possible changes that could be seen when a larger cohort is studied.

# 3. RESULTS

## 3.1 Cross-sectional analysis

*Volume*
As stated in Table 4, patients with MCI had a significantly higher volume of WMHs than normal controls. This difference was still significant when the WMH volume was corrected for white matter volume. Age was significantly correlated with total WMH volume ($r = 0.47$, $p < 0.001$) and total WMH volume corrected for white matter volume ($r = 0.48$, $p < 0.001$). White matter volume was not correlated with WMH volume ($r = -0.06$, $p = 0.379$).

Table 4: WMH volume in NC and MCI subjects.

| | NC | MCI | p-value* |
|---|---|---|---|
| WMH volume ($cm^3$) | 2.74 (0 – 59.51) | 4.95 (0.11 – 167.08) | 0.013 |
| WMH volume (% WM volume) | 0.46 (0 – 9.73) | 0.90 (0 – 29.28) | 0.017 |

* Mann-Whitney-U test
Values indicated in parentheses indicate range

*Spatial distribution*
Lesions are classified according to their distance to the ventricular wall into juxtacortical, periventricular and deep WMHs (Figure 4). Table 5 shows the median WMH volume corrected for white matter volume per class for normal controls and MCI subjects. The difference in volume is statistically significant for the juxtacortical lesions, as well as for the periventricular and deep WMHs. All lesion classes show a correlation with age, as well as a strong correlation with total WMH volume.

Table 5: Juxtacorctical WMH volume, periventricular WMH volume and deep WMH volume in NC and MCI subjects.

| | NC | MCI | p-value* |
|---|---|---|---|
| Juxtacortical (%WM volume) | 0.18 (0 – 2.28) | 0.42 (0 – 3.46) | 0.004 |
| Periventricular (% WM volume) | 0.15 (0 – 4.07) | 0.33 (0 – 16.84) | 0.015 |
| Deep (% WM volume) | 0.08 (0 – 5.45) | 0.12 (0 – 10.83) | 0.040 |

* Mann-Whitney-U test
Values indicated in parentheses indicate range

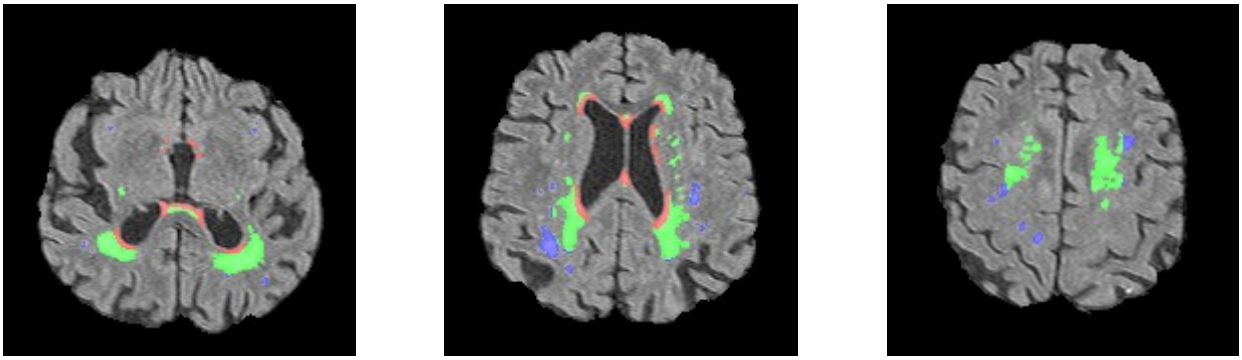

(a) (b) (c)

Figure 4: WMHs are classified according to their distance to the ventricular wall. Juxtaventricular WMHs are indicated in red, periventricular WMHs in green and deep WMHs in blue.

Table 6 shows the voxel-wise WMH volume, corrected for white matter volume, per octant for the NC and MCI group. The WMH volume per octant is corrected for different brain sizes by expressing it as percentage of white matter volume in the same octant. For octant I, II, III, and IV, the voxel-wise volume of WMHs is significantly larger in the MCI group then in the normal controls. There is no difference in voxel-wise WMH volume in octants V, VI, VII and VIII. WMH volume per octant is not correlated with corrected total WMH volume. Only Age is correlated with lesion volume in octant VI.

Table 6: Voxel-wise volume of lesions [% WM volume] per octant.

| | NC | MCI | p-value* |
|---|---|---|---|
| Octant I | 0.52 (0 – 18.41) | 1.49 (0 – 40.99) | 0.005 |
| Octant II | 0.57 (0 – 37.38) | 1.22 (0 – 37.78) | 0.006 |
| Octant III | 0.37 (0 – 15.67) | 0.62 (0 – 41.62) | 0.035 |
| Octant IV | 0.34 (0 – 14.58) | 0.58 (0 – 54.90) | 0.018 |
| Octant V | 0.06 (0 – 12.74) | 0.12 (0 – 38.58) | 0.076 |
| Octant VI | 0.09 (0 – 15.65) | 0.11 (0 – 47.92) | 0.145 |
| Octant VII | 0.43 (0 – 11.79) | 0.69 (0 – 53.79) | 0.080 |
| Octant VIII | 0.47 (0 – 24.69) | 0.68 (0 – 55.63) | 0.065 |

* Mann-Whitney-U test

Values indicated in parentheses indicate range

### 3.2 Longitudinal analysis

*Volume*

Table 7a shows the total WMH volume at baseline and follow up, the matched WMH volume at baseline and follow up and the lost and newly found WMH volume for each subject. The annual change of WMH volume for all four subjects is shown in Table 7b. Although in subjects 3 and 4 a larger volume of WMHs is lost during follow up than is newly found, the total WMH volume increases over time. In subject 1, the total WMH volume also increased, but more new lesions were found at follow up than lost at baseline. When only the matched volume is taken into account, this increase in WMH volume was present in all subjects. For subject 3, the total annual change is negative due to the large volume of lost WMHs. However, the matched WMHs have increased in volume, indicating progression of WMHs. Lost and new WMHs are on average of smaller size (0.029 and 0.014 $cm^3$, respectively) than matched WMHs at baseline (2.85 $cm^3$) and follow up (0.84 $cm^3$).

Table 7: (a) WMH volume [% WM volume] for each subject. Lost lesions are lesions only found at baseline and are therefore expressed as % WM volume at baseline. New lesions are only found at follow up and are expressed as % WM volume at follow up.
(b) Annual change of WMH volume [$cm^3$ per year] for each subject.

(a)

| ID | Total | | Matched | | Lost | New |
|---|---|---|---|---|---|---|
| | Baseline | Follow Up | Baseline | Follow Up | Baseline | Follow Up |
| 1 | 0.05 | 0.11 | 0.03 | 0.08 | 0.01 | 0.03 |
| 2 | 1.19 | 1.58 | 0.96 | 1.54 | 0.22 | 0.05 |
| 3 | 0.29 | 0.27 | 0.16 | 0.26 | 0.13 | 0.00 |
| 4 | 28.27 | 32.64 | 23.34 | 32.43 | 4.93 | 0.21 |

(b)

| ID | Total | Matched |
|---|---|---|
| 1 | 0.07 | 0.06 |
| 2 | 0.51 | 0.70 |
| 3 | -0.03 | 0.22 |
| 4 | 1.32 | 5.73 |

Spatial distribution is described by classifying lesions according to their distance to the ventricular wall. Lost WMHs and newly found WMHs seem to be evenly distributed over the three categories (results not shown). Annual change of WMH volume for each subclass is shown in Table 8. In subjects 1 and 3, both with a low total lesion load, the progression of WMHs predominantly derives from the juxtacortical lesions. In subjects 2 and 4, both with a higher total lesion load, the progression is predominantly based on the periventricular lesions. In subjects 3 and 4, the annual change of deep WMHs is negative.

Table 8: Annual change of WMH volume [$cm^3$ per year] for each subject, subclassified as juxtacortical, periventricular and deep WMHs.

| ID | WMH | Juxtacortical | Periventricular | Deep |
|---|---|---|---|---|
| 1 | All | 0.04 | 0.03 | 0.01 |
| | Matched | 0.02 | 0.02 | 0.02 |
| 2 | All | 0.14 | 0.25 | 0.12 |
| | Matched | 0.20 | 0.31 | 0.19 |
| 3 | All | 0.12 | 0.04 | -0.18 |
| | Matched | 0.18 | 0.01 | -0.1 |
| 4 | All | 0.53 | 1.98 | -1.19 |
| | Matched | 2.63 | 3.31 | -0.21 |

Table 9 shows the voxel-wise change in WMH volume per octant. Although all subjects show a different pattern of WMH progression, there are some similarities. For all subjects, WMH volume change was larger in octants I and IV than in octants II and III. Also, the change in volume is larger in the upper part of the brain (octants I-IV) than in the lower part of the brain (octants V-VIII). The change in volume based on the centre of mass of the lesions is not determined, since this does not represent progression in different brain parts accurately.

Table 9: Annual change of voxel-wise WMH volume [% WM volume per year] for each subject per octant.

| ID | WMH | I | II | III | IV | V | VI | VII | VIII |
|---|---|---|---|---|---|---|---|---|---|
| 1 | All | 0.01 | 0 | -0.001 | 0.02 | 0.01 | 0.03 | 0.001 | 0 |
| | Matched | 0 | 0 | 0 | 0.01 | 0 | 0.03 | 0.005 | 0 |
| 2 | All | 0.42 | 0.04 | 0.007 | 0.09 | -0.03 | 0.08 | 0.02 | 0.02 |
| | Matched | 0.58 | 0.03 | 0.004 | 0.13 | 0.04 | 0.08 | 0.02 | 0.007 |
| 3 | All | 0.06 | 0.006 | -0.007 | 0.06 | -0.06 | -0.005 | -0.01 | -0.12 |
| | Matched | 0.08 | 0.01 | 0.03 | 0.10 | 0 | 0.005 | 0.008 | 0 |
| 4 | All | 1.98 | 0.60 | -0.48 | 1.26 | -0.08 | 0.24 | 0.88 | 0.02 |
| | Matched | 2.56 | 1.56 | 0.56 | 1.87 | 0.64 | 1.31 | 1.86 | 0.83 |

## 4. DISCUSSION

WMHs have been automatically quantified in two different ways. Total volume and spatial distribution are determined and compared between normal controls and MCI subjects.

MCI subjects have a significantly higher juxtacortical, periventricular and deep WMH volume than normal controls. However, these classified volumes are all strongly correlated to the total WMH volume. The same effect was found by DeCarli et al.[7], who suggest that categorical distinctions between periventricular and deep WMHs are arbitrary. Conclusions between causal factors or cognition and subclassified lesion volume might more accurately reflect their relation to total WMH volume than a relation to the subclassified WMH volume.
To compare WMH locations between subjects, an ideal coordinate system is defined in the brain. The yaw, roll and pitch angles are determined to compensate for tilting of the head. The calculation of the roll and yaw angle is based on the bilateral symmetry of the brain. Although Liu et al.[19] show that their method is insensitive to pathologies in the brain, it has also been suggested that AD affects the symmetry of the brain[22]. This method of determining yaw and roll angle might therefore be less accurate for brains affected by AD. However, in this research only normal controls and MCI subjects are studied.
The orientation of the corpus callosum is used in the determination of the pitch angle. The corpus callosum, however, has a relatively inconstant relationship to the central grey matter nuclei[20]. Usage of the corpus callosum to define the pitch angle might therefore have led to variances in the orientation of the ideal coordinate system and consequently to differences in the results.
All significant differences in spatial distribution are situated in the upper half of the brain (octants I-IV). This is in agreement with the literature[23,24], where a predilection for deep periventricular regions, specifically around the frontal and posterior ventricular horns, was found. These regions are situated in the octants I-IV in our ideal coordinate system. However, each octant contains multiple white matter tracts, making it impossible to examine the relationship between the results and the neuroanatomy.

Change of WMH properties in four subjects is determined with the same methods as in the cross-sectional analysis. Although only a small dataset is used, which limits the possibility to draw firm conclusions, the results give an indication of the possible changes. Furthermore, they provide insight into the usefulness of the properties in assessing WMH progression. The results give only an indication of the natural WMH progression due to ageing, since none of the four subjects cognitive ability declined.
The percentage of lost WMH volume is high in subject 3 (72.4%), leading to a decrease in total WMH volume. This could, however, be caused by errors in the segmentation procedure. As is shown by Lopes Simões et al.[14,15], the WMH segmentation algorithm has a low accuracy (DSC = 0.51) when the lesion load is below 10 $cm^3$ Therefore, small lesions segmented in the baseline volume might be missed in the follow up volume.
According to the current literature[18], WMHs originate from the juxtaventricular region and progressively spread out into the white matter. The four analysed datasets support this hypothesis. Subjects 1 and 3, with a low lesion load, show the largest progression in the juxtacortical region, while subjects 2 and 4 show the largest progression in the periventricular region. Subjects 3 and 4 show a decrease in WMH volume in the deep white matter. This might be due to the fact that more lesions are lost than newly found, although this is also the case in subjects 1 and 2.
Progression of WMH volume is more profound in the upper part than in the lower part of the brain. Also, more progression is seen in the frontal part of the brain. This is partly caused by the fact that the total volume of WMHs in the frontal part was larger than in the occipital part. This difference remained when the rate of change was corrected for WMH volume in each octant. This suggests that WMHs in the frontal part of the brain grow more rapidly than WMHs in the occipital part of the brain.
The presented cases show that progression of WMHs occurs even without cognitive changes. This might limit the predictive value of WMHs for cognitive decline, however, more research on a larger cohort is necessary to confirm this. In further research, focus should lie on the change in volume in relation to the spatial location. This can indicate whether progression of WMHs is involved in the development of AD and which brain areas are influenced by WMHs.

## 5. CONCLUSION

From the cross-sectional analysis, it can be concluded that MCI subjects have a significantly higher total volume of WMHs than normal controls. When looking at spatial distribution, MCI subjects have a higher volume of WMHs in the juxtacortical region, as well as in the periventricular and deep white matter. MCI subjects also have a larger WMH volume in the upper half of the brain than normal controls.
Longitudinal analysis suggests that progression of WMHs in subjects with a low lesion load predominantly originates from the juxtacortical lesions, while in subjects with a higher lesion load, progression is caused by periventricular lesions. The four in detail analysed datasets indicated that progression of WMHs is caused by expansion and emergence

of lesions in subjects with a low lesion load, while only grow of pre-existing lesions is responsible for progression in subjects with a high lesion load. Secondly, spatial distribution is evaluated by dividing the brain into eight octants. This suggests that WMHs progress more rapidly in the frontal and upper part of the brain.

## REFERENCES


[1] Petersen, R. C.., others., "Conceptual overview," Mild cognitive impairment: Aging to Alzheimer's disease, 1–14, Oxford University Press New York, NY (2003).

[2] Jack, C. R., Albert, M. S., Knopman, D. S., McKhann, G. M., Sperling, R. A., Carrillo, M. C., Thies, B.., Phelps, C. H., "Introduction to the recommendations from the National Institute on Aging-Alzheimer's Association workgroups on diagnostic guidelines for Alzheimer's disease," 3, Alzheimer's & Dementia **7**(3), 257–262, Elsevier (2011).

[3] Petersen, R. C., Doody, R., Kurz, A., Mohs, R. C., Morris, J. C., Rabins, P. V., Ritchie, K., Rossor, M., Thal, L., et al., "Current concepts in mild cognitive impairment," 12, Archives of neurology **58**(12), 1985–1992, American Medical Association (2001).

[4] Silbert, L. C., Dodge, H. H., Perkins, L. G., Sherbakov, L., Lahna, D., Erten-Lyons, D., Woltjer, R., Shinto, L.., Kaye, J. A., "Trajectory of white matter hyperintensity burden preceding mild cognitive impairment," 8, Neurology **79**(8), 741–747, AAN Enterprises (2012).

[5] De Groot, J. C., De Leeuw, F.-E., Oudkerk, M., Van Gijn, J., Hofman, A., Jolles, J.., Breteler, M., "Periventricular cerebral white matter lesions predict rate of cognitive decline," 3, Annals of neurology **52**(3), 335–341, Wiley Online Library (2002).

[6] Mortamais, M., Reynes, C., Brickman, A. M., Provenzano, F. A., Muraskin, J., Portet, F., Berr, C., Touchon, J., Bonafé, A., et al., "Spatial distribution of cerebral white matter lesions predicts progression to mild cognitive impairment and dementia," 2, PloS one **8**(2), e56972, Public Library of Science (2013).

[7] DeCarli, C., Mungas, D., Harvey, D., Reed, B., Weiner, M., Chui, H.., Jagust, W., "Memory impairment, but not cerebrovascular disease, predicts progression of MCI to dementia," 2, Neurology **63**(2), 220–227, AAN Enterprises (2004).

[8] Ross, E. D., Hansel, S. L., Orbelo, D. M.., Monnot, M., "Relationship of leukoaraiosis to cognitive decline and cognitive aging," 2, Cognitive and behavioral neurology **18**(2), 89–97, LWW (2005).

[9] Schmidt, R., Ropele, S., Enzinger, C., Petrovic, K., Smith, S., Schmidt, H., Matthews, P. M.., Fazekas, F., "White matter lesion progression, brain atrophy, and cognitive decline: the Austrian stroke prevention study," 4, Annals of neurology **58**(4), 610–616, Wiley Online Library (2005).

[10] Schmermund, A., Möhlenkamp, S., Berenbein, S., Pump, H., Moebus, S., Roggenbuck, U., Stang, A., Seibel, R., Grönemeyer, D., et al., "Population-based assessment of subclinical coronary atherosclerosis using electron-beam computed tomography," 1, Atherosclerosis **185**(1), 177–182, Elsevier (2006).

[11] Schmermund, A., Möhlenkamp, S., Stang, A., Grönemeyer, D., Seibel, R., Hirche, H., Mann, K., Siffert, W., Lauterbach, K., et al., "Assessment of clinically silent atherosclerotic disease and established and novel risk factors for predicting myocardial infarction and cardiac death in healthy middle-aged subjects: rationale and design of the Heinz Nixdorf RECALL Study," 2, American heart journal **144**(2), 212–218, Elsevier (2002).

[12] Smith, S. M., "Fast robust automated brain extraction," 3, Human brain mapping **17**(3), 143–155, Wiley Online Library (2002).

[13] Zhang, Y., Brady, M.., Smith, S., "Segmentation of brain MR images through a hidden Markov random field model and the expectation-maximization algorithm," 1, Medical Imaging, IEEE Transactions on **20**(1), 45–57, IEEE (2001).

[14] Simoes, R., Slump, C., Mönninghoff, C., Wanke, I., Dlugaj, M.., Weimar, C., "Automatic histogram-based segmentation of white matter hyperintensities using 3D FLAIR images," SPIE Medical Imaging, 83153K–83153K, International Society for Optics and Photonics (2012).

[15] Simes, R., Mönninghoff, C., Dlugaj, M., Weimar, C., Wanke, I., Walsum, A.-M. van C. van., Slump, C., "Automatic segmentation of cerebral white matter hyperintensities using only 3D FLAIR images," 7, Magnetic resonance imaging **31**(7), 1182–1189, Elsevier (2013).

[16] Jenkinson, M., Bannister, P., Brady, M.., Smith, S., "Improved optimization for the robust and accurate linear registration and motion correction of brain images," 2, Neuroimage **17**(2), 825–841, Elsevier (2002).

[17] Jenkinson, M.., Smith, S., "A global optimisation method for robust affine registration of brain images," 2, Medical image analysis **5**(2), 143–156, Elsevier (2001).

[18] Kim, K. W., MacFall, J. R.., Payne, M. E., "Classification of white matter lesions on magnetic resonance imaging in elderly persons," 4, Biological psychiatry **64**(4), 273–280, Elsevier (2008).
[19] Liu, Y., Collins, R. T.., Rothfus, W. E., Automatic extraction of the central symmetry (mid-sagittal) plane from neuroradiology images, Carnegie Mellon University, the Robotics Institute (1996).
[20] Weiss, K. L., Pan, H., Storrs, J., Strub, W., Weiss, J. L., Jia, L.., Eldevik, O. P., "Clinical brain MR imaging prescriptions in Talairach space: technologist-and computer-driven methods," 5, American journal of neuroradiology **24**(5), 922–929, Am Soc Neuroradiology (2003).
[21] Rohwedder, L. H., "Number of the octants I to VIII of the 3D cartesian coordinate system" (2014).
[22] Illán, I. A., Górriz, J. M., Ramırez, J., Lang, E. W., Salas-Gonzalez, D.., Puntonet, C. G., "Bilateral symmetry aspects in computer-aided Alzheimer's disease diagnosis by single-photon emission-computed tomography imaging," 3, Artificial intelligence in medicine **56**(3), 191–198, Elsevier (2012).
[23] Holland, C. M., Smith, E. E., Csapo, I., Gurol, M. E., Brylka, D. A., Killiany, R. J., Blacker, D., Albert, M. S., Guttmann, C. R., et al., "Spatial distribution of white-matter hyperintensities in Alzheimer disease, cerebral amyloid angiopathy, and healthy aging," 4, Stroke **39**(4), 1127–1133, Am Heart Assoc (2008).
[24] Yoshita, M., Fletcher, E., Harvey, D., Ortega, M., Martinez, O., Mungas, D., Reed, B.., DeCarli, C., "Extent and distribution of white matter hyperintensities in normal aging, MCI, and AD," 12, Neurology **67**(12), 2192–2198, AAN Enterprises (2006).